On the advection of tracer by eddies on the beta-plane: A numerical study

E. S. Benilov

Nonlinear Processes in Geophysics (1999) 6: 67–77

Nonlinear Processes in Geophysics

On the advection of tracer by eddies on the beta-plane: A numerical study

E. S. Benilov

Department of Mathematics, University of Limerick, Ireland

Received: 25 March 1999 – Revised: 09 June 1999 – Accepted: 14 June 1999

Abstract. The evolution of tracer "injected" into an equivalent barotropic eddy on the beta-plane is examined numerically. The eddy is governed by the standard quasigeostrophic equation, and the concentration of tracer is governed by the advection equation with diffusion. At the initial moment of time, the streamfunction and distribution of tracer are both radially or elliptically symmetric. After the first 10-30 days, a spiral-like strip, where the gradient of concentration is large, develops in the tracer field, whereas the eddy remains smooth for a relatively long time. To put this conclusion in quantitative terms, a "tracer variability indicator" is introduced and shown to grow much faster than a similar characteristic of the potential vorticity field (notwithstanding the fact that the tracer concentration and PV satisfy the same governing equation). A simple explanation as to why the tracer is more affected by filamentation than PV is provided for eddies with small Burger number. It is demonstrated that the high-gradient strip develops, unless stopped by turbulent diffusion, into an inversion (non-monotonicity) of the tracer concentration field. Finally, the results of simulations are compared to the spiral patterns in the real-life eddies observed in the East Australian Current.

1 Introduction

The characteristics of oceanic eddies are inherited, to a certain extent, from the frontal current which they have been shed by. Roughly speaking, the profile of an eddy can be obtained by "bending" the frontal current into a circular or elliptic ring. Thus, after breaking free, the velocity, temperature, salinity and other fields of the eddy are close to being radially or elliptically symmetric. Even if there were, initially, asymmetric inhomogeneities of, say, temperature or salinity, they would be rapidly averaged out along all closed streamlines (Rhines and Young, 1983). In the course of further evolution, however, the eddy is affected by sheared currents, β-effect and bottom topography, which distort its shape and cause filamentation. Although it would be natural to assume that all characteristics of the eddy lose smoothness at the same rate, no quantitative studies have been performed to clarify this point[1].

The present paper examines the evolution of quasigeostrophic eddies on the β-plane. The attention is focussed on the equivalent barotropic motion, which is governed by a single dynamic characteristic (the effective depth of the active layer). All other fields (e.g. salinity and temperature at a fixed depth) can be treated as tracers and described, with a reasonable degree of accuracy, by the advection/diffusion equation. Surprisingly, the tracer field develops filamentation much faster than the streamfunction and potential vorticity – despite the fact that the latter is governed by the same equation as the tracer concentration. Physically, the weaker stretching of the active characteristics of the flow occurs because they act back on the velocity field that advects them.

In section 2 of this paper, we shall present the results of simulation of the advection of tracer by circular eddies. It should be emphasised that we are *not* interested in the effect of "spiralisation" of an initial tracer "spot" by a vortex with differential rotation – that one has been examined many times before (see Rhines and Young, 1983; Flohr and Vassilicos, 1997 and references therein). We shall assume that the initial conditions for the vortex and tracer are radially symmetric and concentric, for which the usual 2D dynamics would cause no "spiraling". In other words, the phenomenon that we are looking at is due primarily to the beta-effect.

In section 3, the results will be extended to (initially)

Correspondence to: E. S. Benilov

[1] There have been published, however, several papers on the evolution of tracers in *turbulent* flows, of which the closest to the present work is (Bartello & Holloway 1991).

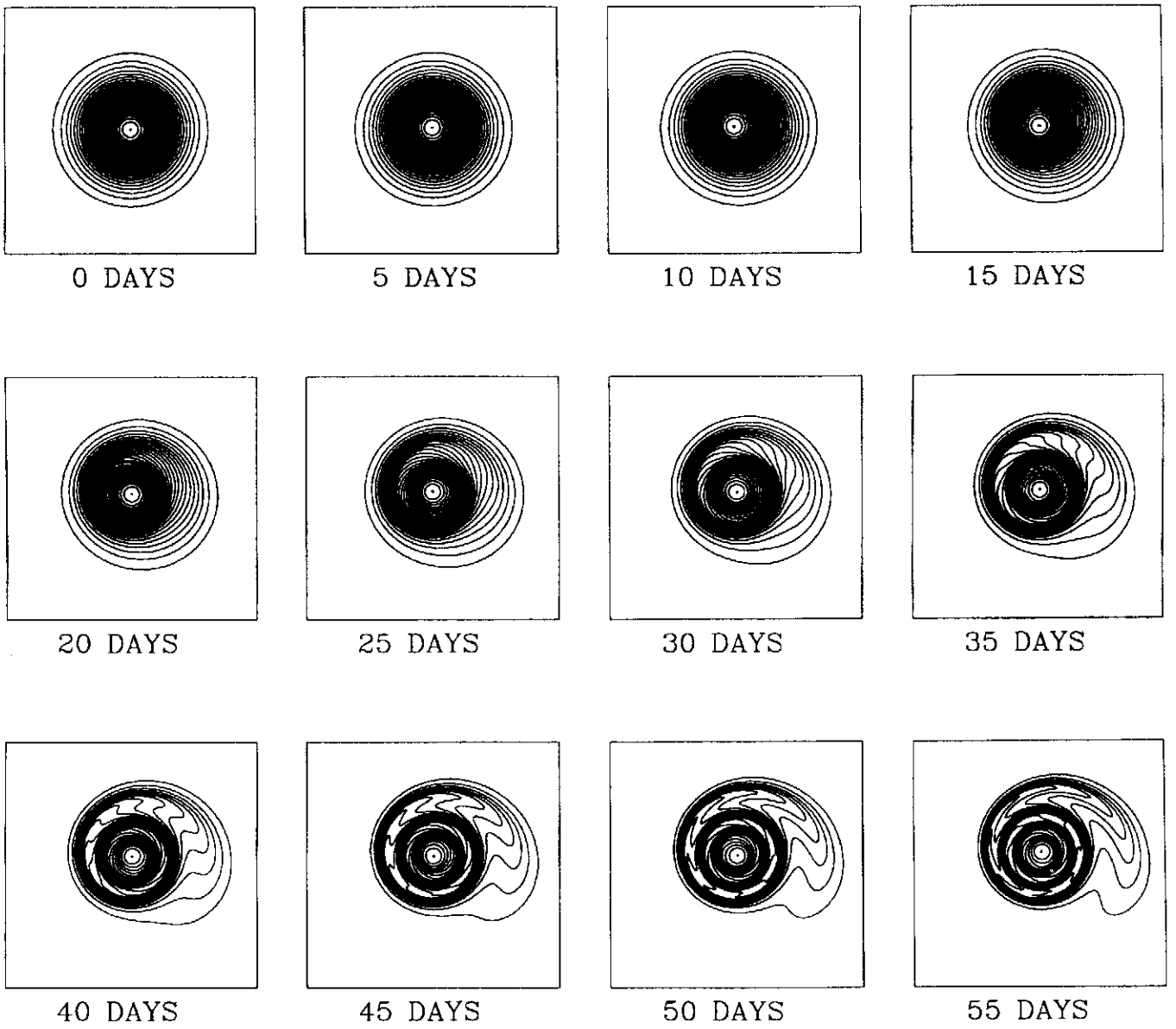

Fig. 1. The evolution of eddy (4): tracer concentration.

elliptic eddies and (initially) elliptic tracer distributions. In section 4, we shall consider the effect of turbulent diffusion and, in section 5, present the conclusions.

2 Circular eddies, non-diffusive model

2.1 Governing equations

The equation describing equivalent barotropic eddies on the β-plane is

$$\frac{\partial}{\partial t}\left(\nabla^2\Psi - \frac{1}{R_d^2}\Psi\right) + J\left(\Psi, \nabla^2\Psi\right) + \beta\frac{\partial\Psi}{\partial x} = 0, \qquad (1)$$

where (x, y, t) are the spatial coordinates and time, Ψ is the streamfunction, R_d is the (internal) deformation radius, β is the meridional gradient of the Coriolis parameter, and J is the Jacobian operator. The concentration $C(x, y, t)$ of the tracer is described by the advection equation:

$$\frac{\partial C}{\partial t} + J(\Psi, C) = 0. \qquad (2)$$

Observe that (2) does not include a diffusive term (the effect of diffusion will be considered in section 4). In all simulations, we used the following values of parameters:

$$R_d = 30\,km, \qquad \beta = 2 \times 10^{-13}\,cm^{-1}s^{-1}$$

(the latter corresponds to the latitude 30°). In this section, we shall consider circular Gaussian eddies:

$$\left.\begin{aligned}\Psi(x, y, 0) &= A\exp\left(-\tfrac{x^2+y^2}{2R^2}\right),\\ C(x, y, 0) &= \exp\left(-\tfrac{x^2+y^2}{2R^2}\right),\end{aligned}\right\} \qquad (3)$$

where A and R are the amplitude and radius of the eddy (the radius of maximum swirl velocity).

2.2 Numerical method

The initial-value problem (1)-(3) was solved using the pseudospectral method with Fourier series and high wavenumber filter for spatial derivatives, and Runge-Kutta fourth-order scheme for time derivatives. The computation domain was a square, with double-periodic boundary conditions. In order to make those "safe", it was made sure that the fastest Rossby wave would propagate, over the simulation time, across no more than 1/3 of the domain size.

A number of conserved quantities were monitored to control the accuracy of simulation: net energy, net mass of the fluid, net mass of the tracer, the extreme potential vorticity and extreme tracer concentration. It turned out that the net characteristics are not indicative of the accuracy: they were conserved with an error of 0.0014% even in those cases where the error in the extreme parameters was greater than 1% (see also subsection 2.4). The experiments showed that a proper resolution of the structure of the tracer field requires an error of less than 0.01% in conservational of the "extreme" parameters – which was achieved by using the resolution of 512×512 gridpoints. Given that in most runs the domain was $500\,km \times 500\,km$, this amounts to approximately one gridpoint per kilometre.

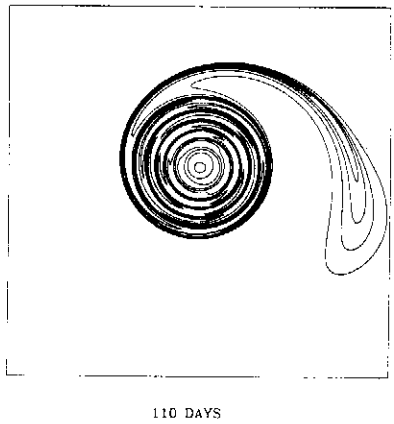

Fig. 2. The final (t = 110 *days*) snapshot of eddy (4): tracer concentration.

2.3 Results

We considered various eddies in the range of 5-30 cm/s for the maximum swirl velocity and 30-100 km for the radius of the vortex – and in all cases observed the same pattern. One case will be described in detail:

$$A = -1.1 \times 10^4\,m^2/s, \qquad R = 50\,km, \qquad (4)$$

which corresponds to a moderate to weak warm-core[2] eddy of maximum velocity of 14 cm/s at a radius of 50 km. The simulation period was 110 days. Soon after the beginning of the evolution, a spiral strip, where the gradient of concentration was large, developed in the tracer field (see Figs. 1. and 2).

Remarkably, nothing similar occurred in the potential vorticity field

$$PV = \nabla^2\Psi - \frac{1}{R_d^2}\Psi + \beta y$$

and streamfunction (see Figs. 3, 4 and 5, 6, respectively) – in fact, both dynamic fields remained close to radially symmetric for a very long time.

The mechanism, giving rise to the spiral pattern, is as follows: some of the particles in the periphery of the eddy spiral slowly towards the centre (this can be seen if the reader superimpose Fig. 1 on Fig. 3). It should be emphasised that the "rotating" component of the particles' trajectories is due to the rotation of the vortex, whereas the motion toward the vortex centre occurs due

[2] Observe that the QG symmetry $\psi \to -\psi$, $y \to -y$ means that the results here equally apply to both warm- and cols-core eddies

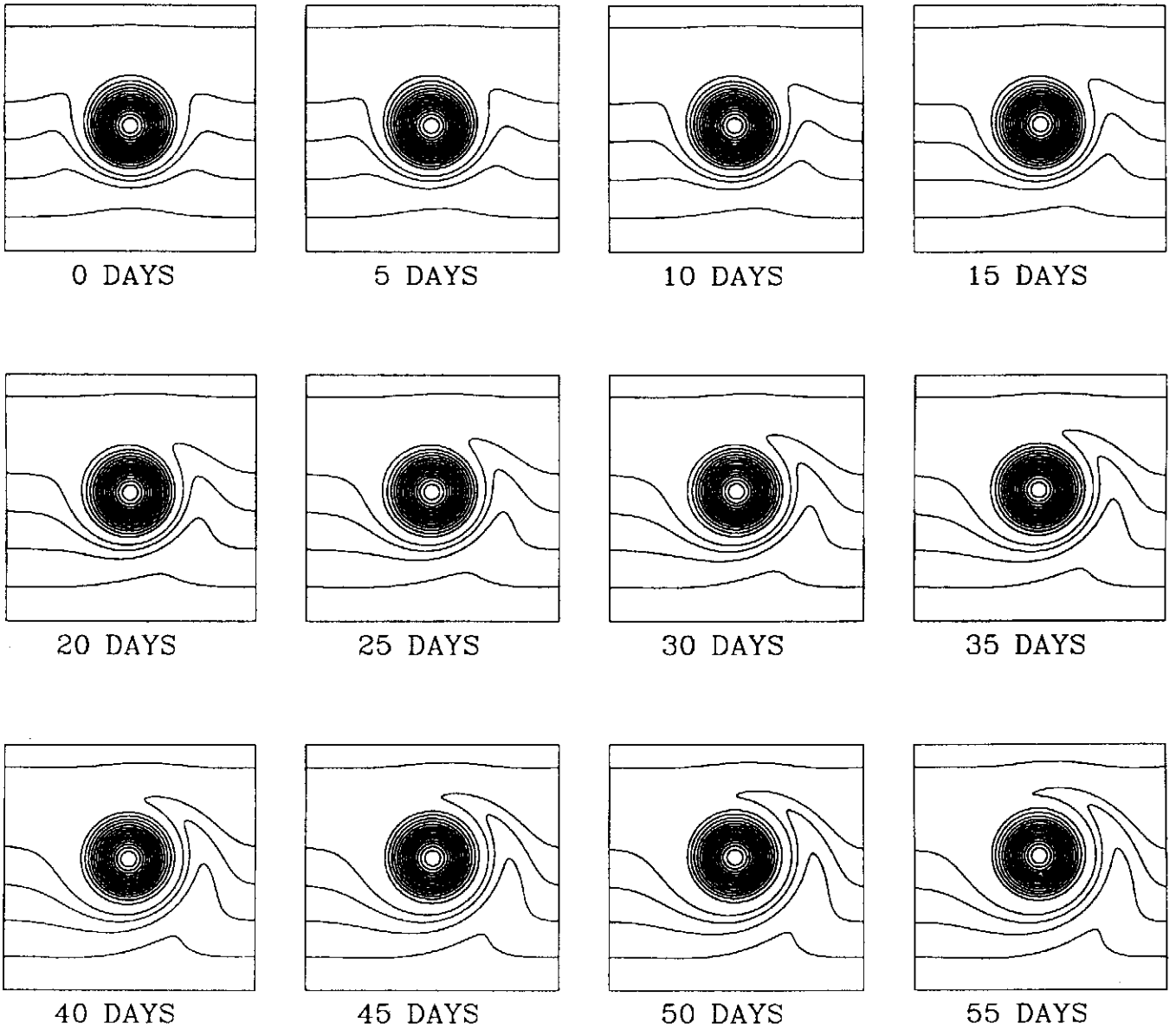

Fig. 3. The evolution of eddy (4): potential vorticity.

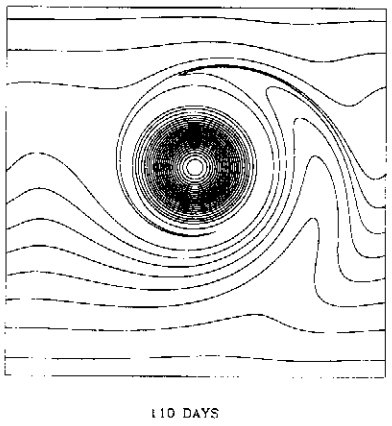

Fig. 4. The final ($t = 110$ days) snapshot of eddy (4): potential vorticity.

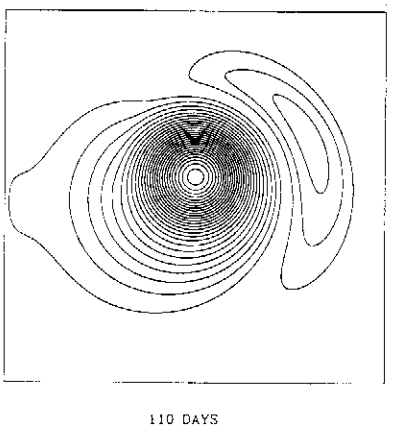

Fig. 6. The final ($t = 110$ days) snapshot of eddy (4): the streamfunction.

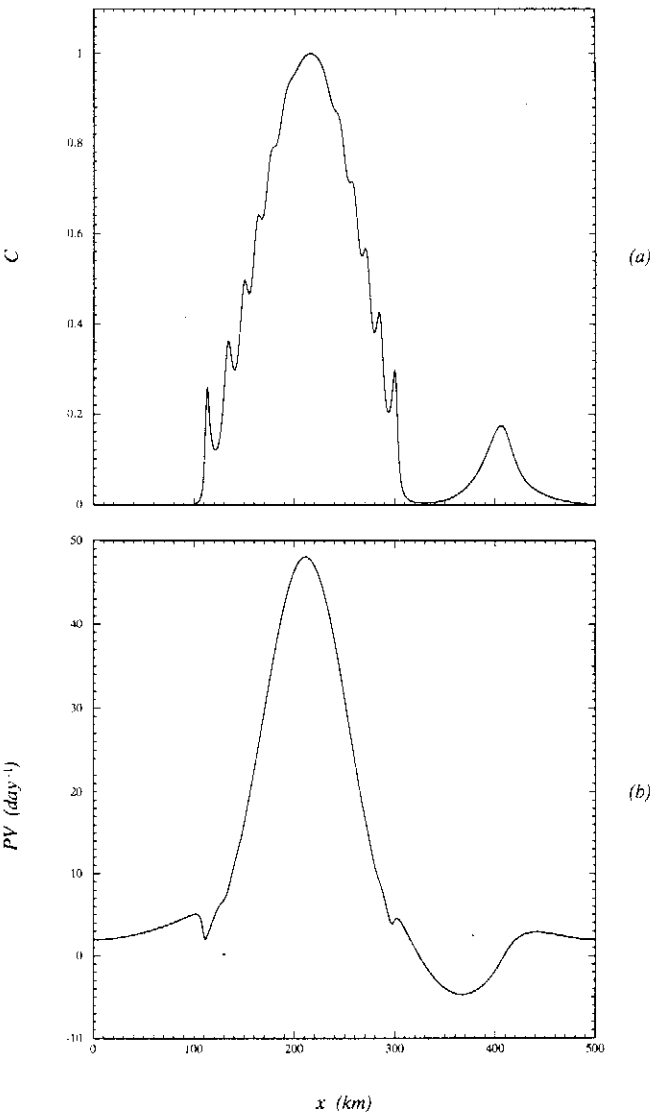

Fig. 7. The cross-section of the final ($t = 110$ days) snapshot of eddy (4).
(a) tracer concentration;
(b) potential vorticity.

to the beta-effect (which is the only radially asymmetric effect).

As a result, particles with high and low values of C end up next to each other, causing high gradients of the concentration field. At later stages of the evolution ($t >$ 60 days), this leads to inversions (non-monotonicity) of the tracer concentration field. Eventually, a tail of particles with high concentration of tracer is "peeled off" the eddy (by the influx of low-C peripheral particles), which agrees with simulations of Dewar and Flierl (1985). Interestingly, the tail is invisible in terms of potential vorticity or streamfunction – compare Figs. 1b,c with 1a (an imaginative reader can still work out how the patterns of C and PV can be reconciled). The inversions and tail can be observed in the zonal cross-section of the concentration field (Fig. 7a). The corresponding PV cross-section, given for comparison in Fig. 7b, is evidently smoother.

In order to put the above observations in quantitative form, the following "variability indicator" was introduced for the tracer concentration field

$$VI_c(t) = \frac{\int\int [\nabla C(x,y,t)]^2 \, dx\, dy}{\int\int [\nabla C(x,y,0)]^2 \, dx\, dy} - 1$$

and compared with a similar quantity, VI_{rv}, calculated for relative vorticity[3]. The results are shown in Fig. 8.

Clearly, the variability of the tracer grows increasingly faster than that of the potential vorticity, despite the fact that the two fields satisfy the same advection equation!

[3]Observe that, in this instance, we compare C with *relative* vorticity, not *potential* vorticity. The reason for that is that the gradient of the latter has a non-zero background value (because of the βy term), which makes VI_{pv} dependent on the computation domain. The variability indicator of relative vorticity is free from this shortcoming and, at the same time, still provides a good estimate of filamentation.

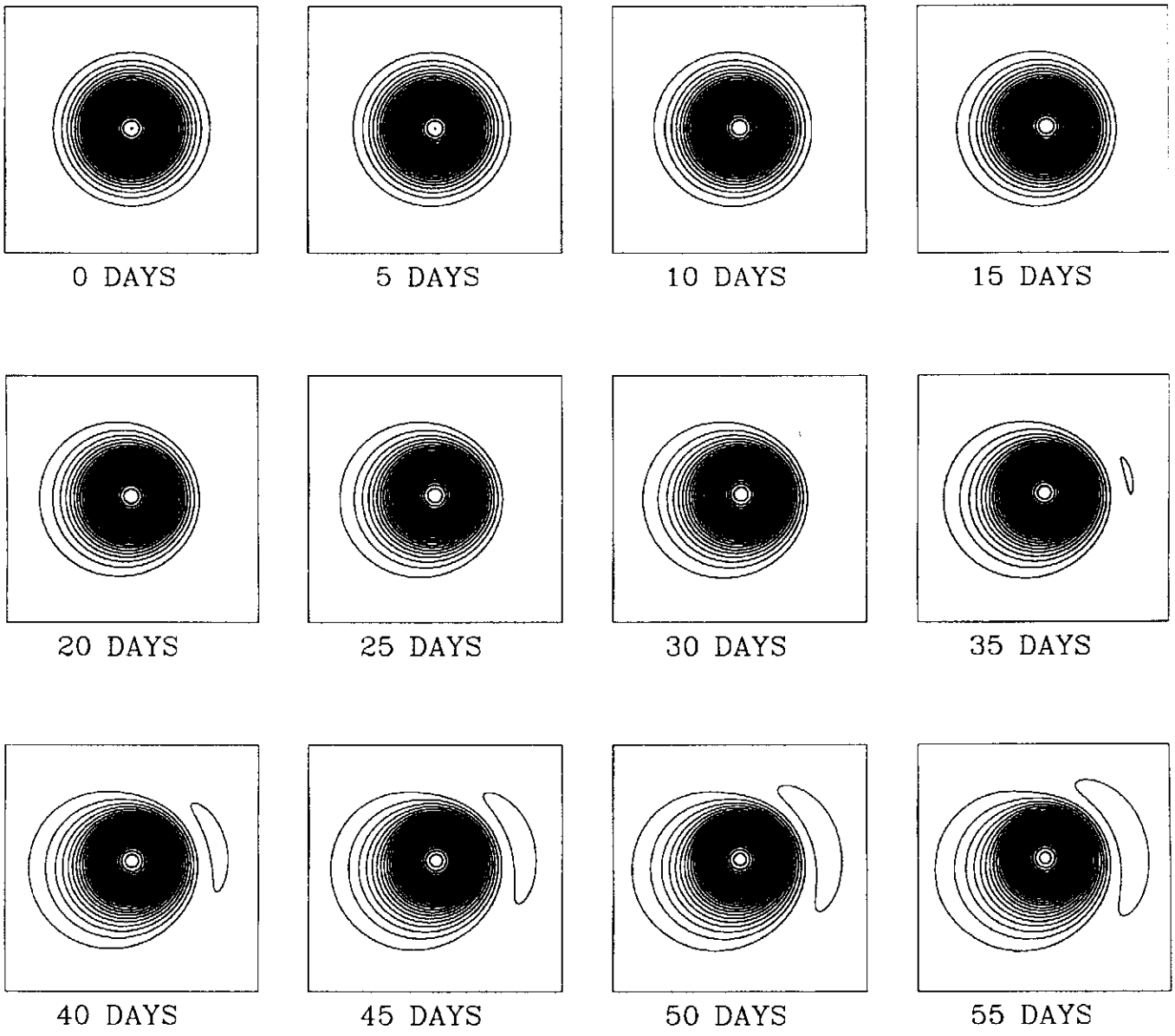

Fig. 5. The evolution of eddy (4): the streamfunction.

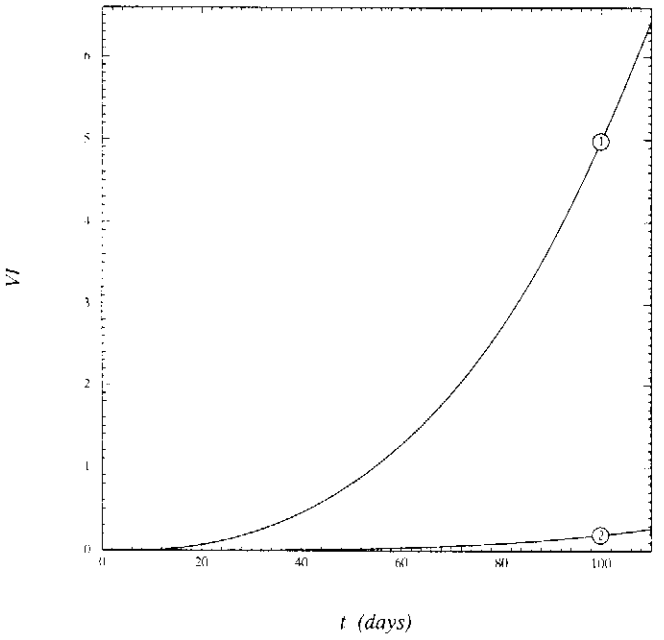

Fig. 8. The "variability indicator" vs. time for eddy (4).
(1) tracer concentration;
(2) potential vorticity.

Finally, we note that the main features of the tracer evolution are *not* sensitive to the initial profile of the vortex or tracer distribution (as long as those remain radially symmetric, of course). Apart from the Gaussian profile, two other profiles were tested, and the behaviours observed were visually indistinguishable from the Gaussian case.

2.4 Discussion

1) Given that C and PV are governed by the same equation, the main issue to be addressed now is what makes their evolution so different.

In order to put this question in a simpler framework, we shall first consider *large*-scale eddies:

$$Bu = \left(\frac{R_d}{R}\right)^2 \ll 1. \tag{5}$$

In this case, the first term in equation (1) is small compared to the second term and thus can be omitted:

$$\frac{1}{R_d^2}\frac{\partial \Psi}{\partial t} + J\left(\Psi, \nabla^2 \Psi\right) + \beta \frac{\partial \Psi}{\partial x} \approx 0. \tag{6}$$

For a radially symmetric initial condition,

$$\Psi(x, y, 0) = \Psi_0(x^2 + y^2),$$

equation (6) can be readily solved:

$$\Psi(x, y, 0) \approx \Psi_0\left[(x - V_R t)^2 + y^2\right]. \tag{7}$$

where

$$V_R = -\beta R_d^2$$

is the speed of long Rossby waves. Thus, until the error introduced by the omission of the small term $\frac{\partial \nabla^2 \Psi}{\partial t}$ "accumulates" and equation (6) fails, the streamfunction distribution of the eddy steadily translates westwards and preserves its shape.

Given condition (5), the expression for potential vorticity can also be simplified:

$$PV \approx \frac{1}{R_d^2}\Psi + \beta y.$$

If rewritten in the form

$$PV \approx \frac{1}{R_d^2}\left(\Psi + V_R\, y\right), \tag{8}$$

this equality demonstrates that the contours of equal potential vorticity coincide with the streamlines, which makes the distribution of PV in the vortex also steady. It should be emphasized that (8) follows from the definition of PV and assumption (5), and thus holds for all initial conditions [as long as they satisfy (5)].

In order to find out if the concentration of tracer is steady, we rewrite equation (2) in the co-moving reference frame

$$x' = x - V_R t, \qquad y' = y, \qquad t' = t$$

and omit the time derivative (and primes):

$$-V_R \frac{\partial C}{\partial x} + J(\Psi_0, C) = 0.$$

This equality can be rewritten in the form

$$C = F\left(\Psi_0 - V_R\, y\right), \tag{9}$$

where the function F is determined by the initial condition for C. Similar to equation (8), this equation seems to suggest that the contours of C coincide with the streamlines. However, *if the initial condition for C is radially symmetric*

$$C(x, y, 0) = C_0\left(x^2 + y^2\right),$$

(9) does not hold for any function F:

$$C_0\left(x^2 + y^2\right) \neq F\left[\Psi_0\left(x^2 + y^2\right) - V_R\, y\right].$$

Thus, the difference in the initial conditions accounts for the difference in the behaviour of PV and C – after all, if the governing equations coincide, the initial conditions can be the only source of distinction.

Observe that, although the Burger number was not all that small in our simulations ($Bu = 0.36$), solution (7) agrees well with what we see in Figs. 1c, 2c. Indeed, the evolution of the eddy is relatively slow – it steadily translates westwards[4], but the initial shape of its core remains virtually unperturbed. In order to determine

[4] The reference frame in all figures is linked to the x-coordinate of the centre of the eddy, which makes the westward translation invisible. It is also worth noting that the meridional drift of the vortex in all case considered was fairly weak.

Table 1. The ratio of variability indicators vs. radius of the eddy after 110 days.

	$R(km)$	Bu	VI_c/VI_{rv}
(4)	50	0.36	23.7
(10)	40	0.56	9.6
(11)	30	1.00	4.6
(12)	20	2.25	1.8

for which values of Bu we should expect qualitatively different behaviours of C and PV, we considered warm-core eddies with the following parameters:

$$A = -0.88 \times 10^4\, m^2/s, \qquad R = 40\, km, \tag{10}$$

$$A = -0.66 \times 10^4\, m^2/s, \qquad R = 30\, km, \tag{11}$$

$$A = -0.44 \times 10^4\, m^2/s, \qquad R = 20\, km \tag{12}$$

and compared them to eddy (4) (observe that all four eddies have the same maximum velocity, 14 cm/s). The results are presented in Table 1

– they suggest that the qualitative difference between the behaviours of C and PV disappears for $R < 30\, km$. Given that most, if not all, oceanic rings are larger than 40 km (Olson, 1991), we conclude that the above argument is fully applicable to the real ocean.

2) In order to check the accuracy of our numerical method, we performed three runs with weaker resolution: 64×64, 128×128 and 256×256 gridpoints, and compared the results with the 512×512 run (see Fig. 9).

Evidently, only the two high-resolution runs can be trusted. In fact, the 64×64 run shows no traces of the spiral structure whatsoever, and the 128×128 run resolves only the two strongest inversions of the tracer concentration in Fig. 7a. Interestingly enough, the two low-resolution runs showed excellent conservation of the net quantities (energy, mass, etc.) – all errors were less than 0.01%. Even the errors in conservation of the extreme quantities look reasonable (1.2% for the 128×128 run). It seems that, in this kind of problem, trustworthy results are guaranteed only if *all* errors of conserved quantities are less than 0.01%.

3) Finally, we note that spiral patterns similar to those simulated here have been observed in the real ocean and, in particular, in the East Australian Current (George Cresswell, private communication - see Fig. 10).

It cannot be claimed with the hundred percent certainty, of course, that the mechanism of formation of these patterns is as described in this paper. In order to deduce a convincing conclusion in this issue, one needs to analyse the velocity field associated with the sea-surface temperature observed. The crucial point here would be the existence of a weak inflow of peripheral water spiraling towards the centre of the eddy, which was always present in our simulations.

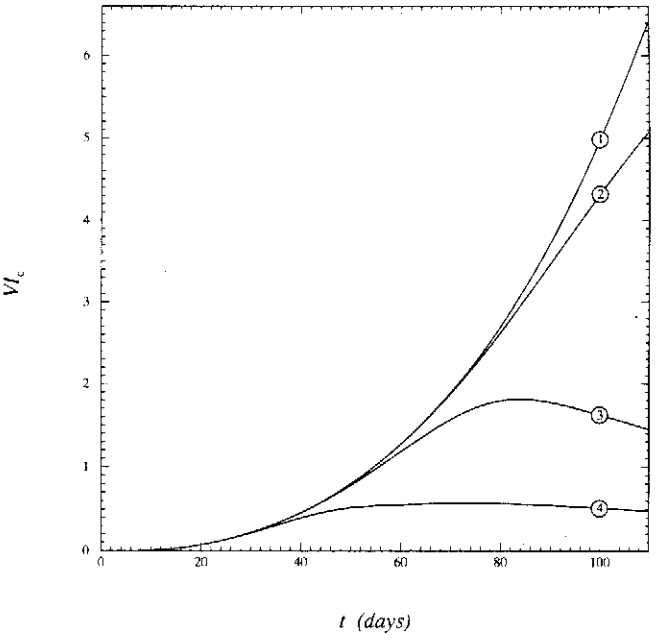

Fig. 9. The "variability indicator" of C vs. time, for eddy (4).
(1) 512×512 gridpoints;
(2) 256×256 gridpoints;
(3) 128×128 gridpoints;
(4) 64×64 gridpoints.

Fig. 10. A satellite image of an eddy in the East Australian Current (the sea surface temperature).

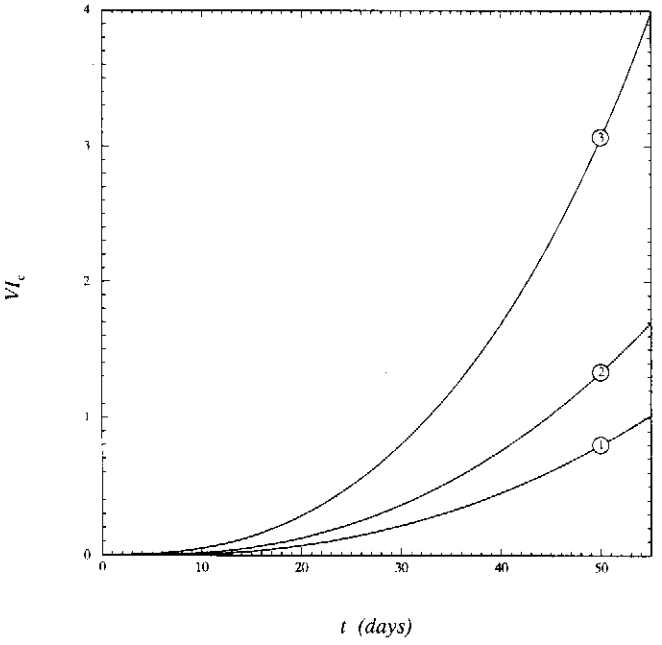

Fig. 11. The "variability indicator" of C vs. time, for
(1) eddy (14) (aspect ratio 1);
(2) eddy (15) (aspect ratio 1.1);
(3) eddy (16) (aspect ratio 1.2).

3 Elliptic eddies

As a first step towards a more realistic approximation of oceanic eddies, we considered elliptic eddies described by

$$\left.\begin{aligned}\Psi(x,y,0) &= A\exp\left(-\tfrac{x^2}{2R_x^2}-\tfrac{y^2}{2R_y^2}\right),\\ C(x,y,0) &= \exp\left(-\tfrac{x^2}{2R_x^2}-\tfrac{y^2}{2R_y^2}\right),\end{aligned}\right\} \tag{13}$$

where A is the amplitude of the eddy, and R_x and R_y are, basically, the major axes of the ellipse. We performed three simulations of eddies of the same amplitude and "average" radius $(R_x + R_y)/2$, but different aspect ratios:

$$\left.\begin{aligned}&A = -1.1\times10^4\, m^2/s,\\ &R_x = 50\, km, \qquad R_y = 50\, km;\end{aligned}\right\} \tag{14}$$

$$\left.\begin{aligned}&A = -1.1\times10^4\, m^2/s,\\ &R_x = 47.5\, km, \qquad R_y = 52.5\, km;\end{aligned}\right\} \tag{15}$$

$$\left.\begin{aligned}&A = -1.1\times10^4\, m^2/s,\\ &R_x = 45\, km, \qquad R_y = 55\, km\end{aligned}\right\} \tag{16}$$

(the maximum velocity in all three cases is close to 15 cm/s). The results are shown in Fig. 11 – clearly, more eccentric eddies are more affected by filamentation than less eccentric eddies.

It should also be noted that spiral patterns and inversions develop in elliptic eddies noticeably faster than those in circular eddies (compare Fig. 12 with Fig. 7a).

The greater susceptibility to filamentation of tracer in elliptic vortices (as opposed to that in circular vortices) appears to be natural at an intuitive level, However, it is not clear how it can be explained in quantitative terms.

4 The effect of turbulent diffusion

Looking at the cross-section of the tracer concentration shown in Fig. 7a, one cannot escape the feeling that turbulent diffusion, if taken into account, would affect strongly the fine structure of the tracer field. It is obvious, in fact, that – sooner or later – the effect of diffusion will smooth all filaments out, and the question is not "whether this occurs", but "when" – before the spiral pattern has developed or after that. But, in either case, the tracer will eventually be homogenized within the eddy's closed streamlines (Rhines and Young, 1983).

In order to clarify, at which stage of the evolution the effect of diffusion becomes important, we estimate the characteristic time of the diffusion

$$\tau_\eta = \frac{L^2}{\eta},$$

where L is the width of the high-gradient area, and η is the turbulent diffusivity. The latter is one of the most uncertain oceanic parameters: it is believed to vary in the range of $10^5 - 10^8\, cm^2/s$ for meso- to large-scale motions (e.g. Pedlosky, 1987). In our case, L is 20-5 km (for the spiral pattern and inversions of C, respectively). Assuming that the diffusivity grows with spatial scale of the tracer distribution[5], we conclude that, in our case, η should be of the order of the lower boundary of the above-mentioned range, $\eta = 10^5\, cm^2/s$ (which agrees, in fact, with the measurements of Ozmidov, 1968; Okubo and Ozmidov, 1970). Estimating τ_η for $L = 20\, km$, we obtain $\tau_\eta = 462\ days$; and for $L = 5\, km$, we obtain $\tau_\eta = 29\ days$. Thus, for the above value of η,

– turbulent diffusion has no influence on the spiral pattern,

– but should affect the inversions of the tracer concentration field.

In other words, the effect of diffusion may prevent high-gradient areas from developing into inversions.

These conclusions have been verified numerically by replacing the advection equation (2) with

$$\frac{\partial C}{\partial t} + J(\Psi, C) = \eta\nabla^2 C \tag{17}$$

and simulating the initial-value problem (1), (17), (13) with $\eta = 10^5\, cm^2/s$. For all eddies, both circular and elliptic, the first stage of evolution (when the spiral

[5] It is implied that turbulent diffusion is created by turbulent motions of scales that are smaller than the spatial scale of the tracer. Thus, smooth (large-scale) distributions of tracer are affected by a *wider* spectrum of turbulence and therefore have *larger* diffusivity.

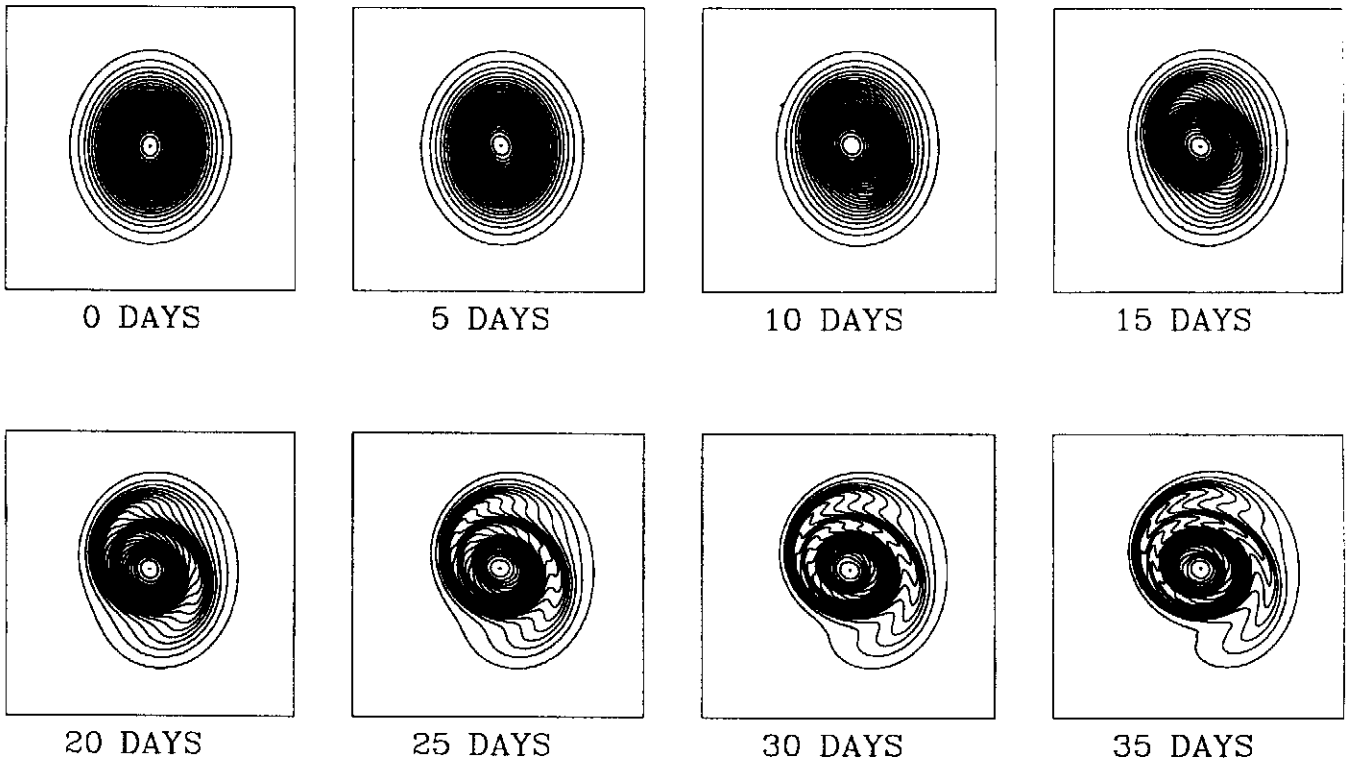

Fig. 12. The evolution of tracer in (elliptic) eddy (16).

pattern develops) was hardly distinguishable from the non-diffusive case. Even for a larger diffusivity, $\eta = 10^6\, cm^2/s$, the spiral pattern was clearly visible in all numerical experiments. However, only elliptic eddies developed inversions of C, and even those did not develop *all* of the fine structure of the non-diffusive case – see the cross-section of the eddy with

$$\left.\begin{array}{l} A = -1.1 \times 10^4\, m^2/s, \\ R_x = 35\, km, \qquad R_y = 70\, km; \end{array}\right\} \tag{18}$$

shown in Fig. 13 (the maximum velocity in this eddy is about 20 cm/s).

The profile of C in circular eddies in all numerical experiments remained monotonic (apart from the non-monotonicity caused by the tail).

It should be noted, however, that these results are not very reliable due to uncertainty in the value of η. Moreover, the whole "differential" approximation of the diffusion term is not a very good model for our case. Generally speaking, turbulent diffusion at meso-scales occurs due to inertial/internal waves 1-15 km long. In our case, the wavelengths of those are comparable to the spatial scale of the tracer field, which clearly makes the differential approximation inapplicable.

In order to model the effect of turbulent diffusion in a tracer field with a spatial scale of 5-20 km, one should use the primitive equations. The diffusivity should be chosen as determined by medium- to short-scale wave turbulence. Longer waves (with wavelengths, say, greater than 5 km) should be included in the initial condition, so the turbulent diffusion will occur "naturally". Observe that this model requires the same kind of resolution (1 gridpoint per kilometre) as the QG-

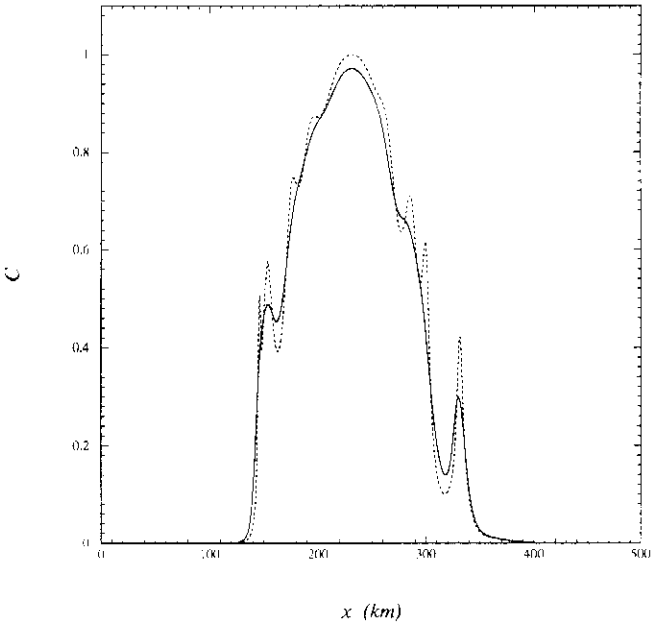

Fig. 13. The cross-section of the concentration field for eddy (18) after 35 days. The solid/dotted lines show the profiles computed using the diffusive/non-diffusive models, respectively.

based model used above.

5 Conclusions

Thus, it has been demonstrated that the concentration of tracer advected by an eddy on the β-plane is affected by filamentation much stronger than the dynamic characteristics of the eddy (streamfunction and PV). A spiral-like strip, where the gradient of concentration is high, develops in the tracer field. Later on, the strip develops – unless stopped by turbulent diffusion – into an inversion (non-monotonicity) of the tracer concentration filed. Elliptic eddies manifest this pattern faster and stronger than circular eddies.

The observed behaviour has been explained theoretically for large-scale eddies, i.e. such that $Bu = (R_d/R)^2 \ll 1$ (where R_d is the deformation radius and R is the radius of the eddy). Numerical experiments suggest that the qualitative difference between the behaviours of C and PV disappears for eddies with $R < 30\,km$. Given that most , if not all, oceanic rings are larger than 30 km (e.g. Olson, 1991), we conclude that our results are fully applicable to the real ocean. In fact, spiral patterns similar to those computed in this paper *have* been observed in the real ocean (George Cresswell, private communication – see Fig. 10), although one cannot claim with certainty that they are a result of the mechanism discussed in this paper.

Finally, we note that all the conclusions obtained in this paper are applicable to an early stage of vortex evolution, when the Rossby-wave radiation has not yet significantly weakened the vortex. In order to examine the later stage, one needs to improve the resolution of the numerical method used by the order of magnitude.

Acknowledgements. This work was supported by the Australian Research Council.

I am grateful to Gregory Reznik for helpful discussions, to George Cresswell who provided the satellite images shown in Fig. 10, and to Roger Grimshaw and George Sutyrin who have independently drawn my attention to solution (7).

References

Bartello, P. and Holloway, G., Passive scalar transport in β-plane turbulence, *J. Fluid Mech.*, *223*, 521-536, 1991.

Dewar, W. K. and Flierl, G. L., Particle trajectories and simple models of transport in coherent vortices, *Dyn. Atmos. Oceans*, *9*, 215-252, 1985.

Flohr, P. and Vassilicos, J. C., Accelerated scalar dissipation in a vortex, *J. Fluid Mech.*, *348*, 295-317, 1997.

Olson, D. B., Rings in the ocean, *Annu. Rev. Earth Planet. Sci.*, *19*, 283-311, 1991.

Ozmidov, R. V., On the dependence of horizontal diffusivity in the ocean on the spatial scale, *Acad. Nauk SSSR, Izv. Atmos. Ocean. Phys.*, *4*, 1224-1225, 1968.

Okubo, A. and Ozmidov, R. V., Empirical dependence of horizontal turbulent diffusivity in the ocean on the spatial scale, *Acad. Nauk SSSR, Izv. Atmos. Ocean. Phys.*, *6*, 534-536, 1970.

Pedlosky, J., *Geophysical Fluid Dynamics*, Springer-Verlag, 1987.

Rhines, P. B. and W. R. Young 1983. How rapidly is a passive scalar mixed within closed streamlines? *J. Fluid Mech.*, *133*, 133-145.